Dynamic Voltage Behavior of a PEM Electrolyzer Under Continuous on/off Loading Cycles Using an Equivalent Circuit Model

Ángel Hernández-Gómez, Diego Langarica-Cordoba, Panfilo Martinez-Rodriguez, Damien Guilbert, Victor Ramirez, Belem Saldivar

Dynamic Voltage Behavior of a PEM Electrolyzer Under Continuous on/off Loading Cycles Using an Equivalent Circuit Model

Ángel Hernández-Gómez, *Member, IEEE,* Diego Langarica-Cordoba, *Senior Member, IEEE,* Panfilo R. Martinez-Rodriguez, *Senior Member, IEEE,* Damien Guilbert, *Senior Member, IEEE,* Victor Ramirez, Belem Saldivar

***Abstract*—Mathematical modeling plays a crucial role in the design and performance evaluation of proton exchange membrane (PEM) electrolyzers. Among the various approaches reported in the literature, equivalent circuit models (ECMs) stand out for their simplicity and suitability for studying voltage behavior and interaction with power electronic interfaces. However, the dynamic voltage response of PEM electrolyzers under continuous on/off loading cycles has not been extensively explored. This paper presents a static–dynamic ECM model that accurately describes the voltage response of a PEM electrolyzer subjected to continuous on/off loading cycles in the supply current, represented by square-wave variations. The model parameters are derived from experimental data and validated through laboratory measurements. Thanks to this model, it is possible to have a better understanding of the PEM electrolyzer voltage behavior when intermittent power sources, such as energy conversion systems, are considered.**

***Index Terms*—Equivalent circuits, Dynamical systems, Hydrogen Storage**

I. Introduction

In recent years, several investments have been reported in large-scale hydrogen production. This is due to its abundance and benefits as a primary energy source. Consequently, the global demand for hydrogen is expected to increase dramatically in the near future [1]. It is estimated that by 2050, water electrolysis will account for more than 60% of global hydrogen production and, although electrolyzers currently only produce 0.3 gigawatts (GW) worldwide, their capacity will reach 850 GW and 3,600 GW for 2030 and 2050, respectively. In addition, it is considered that 95% of the energy sources for the operation of the electrolyzers will be of renewable energy sources supplied by electronic converters [2]. The primary function of the electrolyzers is to carry out water electrolysis in an efficient way for green hydrogen production. Compared with anion exchange membrane and solid oxide electrolyzers, proton exchange membrane (PEM) and alkaline electrolyzers are the most technologically developed, already reaching the commercial stage [3]. However, between these two technologies, the PEM electrolyzer has shown higher performance due to its applicability advantages, such as its operational flexibility, compact design, higher energy density, and high-purity hydrogen production [4].

Due to the phenomena that occur during the operation of the electrolyzer when powered by renewable energy sources, mathematical modeling plays a vital role in its research and development [5]. Therefore, using this theoretical tool, it is possible to examine control and failure analysis, energy management, and optimization of the PEM electrolyzer [6], [7]. Models of different complexity have been developed for the research on PEM electrolyzers, which can be classified as: analytical, empirical or semi-empirical, and mechanistic. Usually, analytical models determine the effect of the main variables on the performance of the electrolyzer [8]. Empirical models are characterized by using experimental data to determine the values of the parameters of the model equations. However, it must be taken into consideration that these models are limited to a specific electrolyzer [9]. Compared to the other two types of models, the mechanistic models are more complex as they use differential and algebraic equations to describe the electrochemical phenomena that occur in the electrolyzer. These models reliably predict the different variables of the PEM electrolyzer. However, mechanistic models need more extensive computations, and, therefore, simulations require a significant amount of time and more sophisticated computer equipment [10].

Among the mechanistic models are the dynamic models, which are useful to describe the behavior of systems in real-time when coupled with renewable energy sources. Although dynamic models for PEM electrolyzers have already been reported in the literature [11], [12], few dynamic models have been developed to describe the voltage behavior of the PEM electrolyzer. To cope with this issue, some authors have modeled the PEM electrolyzer voltage dynamics using an equivalent electric circuit model (ECM). In general for PEM electrolyzers, a capacitor is used to model the electrical double-layer phenomenon [13]. In [14], an ECM has been developed for a single-cell PEM electrolyzer under steady-state conditions, taking into account useful power conversion and electrolyzer losses. In addition, the model parameters have been calculated as functions of temperature and pressure. In [15], a detailed method of electrochemical impedance spectroscopy has been applied to identify ohmic, activation, and mass transfer losses.

Ángel Hernández-Gómez and Panfilo R. Martinez-Rodriguez are with the School of Sciences, Universidad Autonoma de San Luis Potosi, SLP 78295, Mexico (e-mails: angel.hernandez@uaslp.mx, pamartinez@ieee.org)

Diego Langarica-Cordoba (corresponding author) is with the Department of Electrical and Computer Engineering, The University of Texas at El Paso, TX 79968, USA (e-mail:dlangaricacordoba@utep.edu)

Damien Guilbert is with the GREAH, Université Le Havre Normandie, Le Havre 76600, France (e-mail:damien.guilbert@univ-lehavre.fr)

Victor Ramirez is with the Department of Renewable Energy, Centro de Investigación Científica de Yucatán (CICY), Yucatán 97205, Mexico; and with the SECIHTI, Mexico City 03940, Mexico; (e-mail:victor.ramirez@cicy.mx)

Belem Saldivar is with the Department of Automatic Control, CINVESTAV-IPN, Mexico City 07360, Mexico (e-mail:belem.saldivar@cinvestav.mx)

Thus, the authors have developed an ECM considering these losses. In [16], the authors have modeled the electrochemical behavior of the PEM electrolyzer using the Randles-Warburg cell as the ECM impedance method. In addition, the current interruption method has been applied to determine the model parameters. This approach comprises two stages: the natural voltage response method, which represents the ohmic losses, and the current switching method, which accounts for the activation and concentration losses. Furthermore, it has been shown that the increase in temperature and electric current significantly decreases the concentration loss. In [17], apart from developing an ECM, it has been shown that ohmic resistance is a critical parameter that can significantly affect the overall performance of the PEM cell, and therefore, its minimization is suggested. The authors in [18] have developed an ECM to design and build a dynamic emulator for the PEM electrolyzer voltage. In addition, the capacitance produced in a PEM electrolyzer composed of three cells has been studied when subjected to sudden changes in the input electrical current. In [19], [20], by using an ECM and different electrical input currents, the authors have developed an adaptive static-dynamic electrical model for the voltage of the PEM electrolyzer and the cells that comprise it. Furthermore, these works have shown that the parameters must be adjusted depending on the input current. In [21], the dynamic behavior of an ECM has been taken into account to design the control system applied to a stacked interleaved buck converter, which supplies the PEM electrolyzer with low-ripple electrical currents and ensures its reliable operation. The authors in [22] have designed a control model to maintain the internal operating temperature of the PEM electrolyzer to improve the electrolysis efficiency and the hydrogen production rate. For designing the control model, the authors have considered the dynamic influence of variables such as the produced hydrogen and oxygen, and the voltage-current behavior, the latter using an ECM.

Due to the importance of ECM for the dynamic study of the PEM electrolyzer voltage, this work analyzes and applies a static-dynamic ECM to the PEM electrolyzer voltage when subjected to continuous disturbances. Unlike existing literature that focuses on steady-state variations or isolated step-changes, this study investigates the response under continuous and rapid on/off loading cycles. To achieve this, the input current is supplied as a square wave with different frequencies and magnitudes, simulating the aggressive switching regimes typical of power electronic interfaces and intermittent renewable energy sources [23], which are usually used to supply energy to PEM electrolyzers. The main contributions of this work are:

- Characterization of the interaction between the double-layer capacitance and charge transfer resistance under continuous switching, providing a more accurate prediction of voltage peaks and operational stress.
- Validation of the proposed ECM using rigorous statistical tests (relative, mean, mean squared, and root mean squared errors) compared to experimental data from a QL-300 PEM electrolyzer.
- An in-depth analysis of how continuous electrical disturbances affect voltage behavior, offering a foundational model for designing robust control strategies in renewable energy applications.

This work is structured in six sections. After discussing the state-of-the-art in the Introduction, a brief explanation of the operation of the PEM electrolyzer and a detailed description of the experimental platform are presented in Section II. Section III describes the development of the static-dynamic model based on an ECM for PEM electrolyzer voltage. Subsequently, the estimated parameters of the proposed model are provided in Section IV. Section V presents numerical simulations of the model with the estimated parameters and its validation through tests; a discussion of this work is also presented in this section. Finally, the conclusions of this research work are summarized in Section VI.

II. Experimental test set-up

A. PEM electrolyzer basic operation

The PEM electrolyzer is an electrochemical device that produces hydrogen and oxygen through the electrolysis process. Generally, a PEM electrolyzer system is composed of two chambers (anode and cathode), a PEM located in the center of the electrolyzer, and an external circuit connected to a DC power source. Each component of the PEM electrolyzer system has a basic function: at the anode, oxygen, electrons, and protons are generated; the membrane is responsible for passing the protons produced to the cathode side; the external circuit flows the electrons from the anode to the cathode; at the cathode, electrons reduce protons, producing hydrogen [24], [25]. In particular, the QL-300 PEM electrolyzer stack utilizes a platinum catalyst and a solid polymer electrolyte membrane, eliminating the need for hazardous liquid electrolytes [26]. The reactions that take place in the anode, cathode, and in general the entire QL-300 PEM electrolyzer system are presented in (1) and its schematic is presented in Figure (1).

$$\begin{aligned} &2H_2O \rightarrow 4H^+ + O_2 + 4e^- \text{ (Anode reaction)},\\ &4H^+ + 4e^- \rightarrow 2H_2 \text{ (Cathode reaction)},\\ &2H_2O \rightarrow 2H_2 + O_2 \text{ (General reaction)}. \end{aligned} \tag{1}$$

Despite having a higher specific energy consumption ($kWh \cdot Nm^{-3}$) compared to the alkaline electrolyzer, the PEM electrolyzer is a promising technology due to its wide operating range, fast response capacity, high current densities ($2\ A{\cdot}cm^{-2}$), and its good performance when coupling with renewable energy sources [27]. This last advantage of the PEM electrolyzer has caught the attention of researchers, as it can cope with the fluctuations of these intermittent power sources by carrying out partial load [28].

B. Dynamic issues

For the development of the experimental tests presented in this work, the PEM electrolyzer QL-300 [29] is employed, Table I shows its characteristics. It is worth noting that this PEM electrolyzer system features its own AC-DC power supply. However, for characterization purposes, it has been removed and substituted by the DC power supply described below.

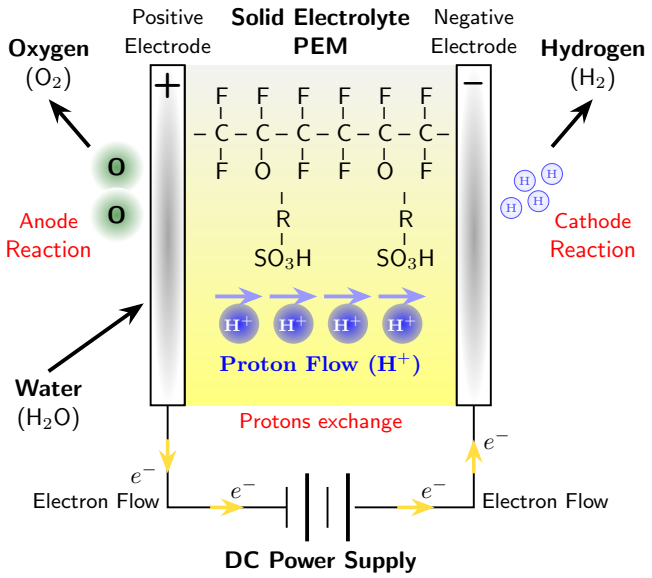

Fig. 1. Basic operation of the QL-300 PEM electrolyzer [26].

TABLE I
SPECIFICATIONS OF THE PEM ELECTROLYZER QL–300 [29].

Parameter	Value	Unit
Hydrogen purity	≥99.999	%
Hydrogen output flow volume range	0–310.3	mL· min^{-1}
Output pressure range	0.2–4	bar
Pressure stability	<0.01	bar
Electrical power range	0–150	W
Dimensions (L×W×H)	(4.2, 2.27, 3.52)	cm
Maximum machine weight	15	kg
Operating voltage range	1.4–2.5	V
Current range	0–60	A
Cell number	1	–
Active area section	150	cm^2
Solid Polymer Electrolyte (SPE)	183	μm

To analyze the behavior of the PEM electrolyzer voltage when subjected to electric currents from intermittent energy sources, the experimental test described below was proposed by the authors to collect experimental data during on/off cycles. Figure 2 shows the equipment and setup to carry out the experimental measurements of voltage and current for a collection time of 4000 seconds. For developing the experiment, the following equipment is employed:

1) A computer with Matlab–Simulink.
2) A DS1104 controller board of dSPACE Company.
3) An oscilloscope MDO34–1000 of Tektronix Company.
4) A voltage sensor.
5) A PEM electrolyzer QL–300.
6) A signal converter of the dSPACE control board to the DC power supply.
7) An electrical current sensor.
8) A DC power supply EL 9160–100 of Elektro Automatick (EA) Company.

The experiments in this work were performed as follows: a square waveform signal was programmed for the dSPACE controller using Matlab-Simulink; the dSPACE controller board sends this signal to the DC power source through a signal converter; the DC power source feeds directly the PEM electrolyzer with a pure DC; the oscilloscope allows recording the database of the measurements of the voltage and electric current sensors of the PEM electrolyzer. Subsequently, the saved database is analyzed. To observe the behavior of the electrolyzer over a sufficiently large time window, each experimental test performed has a duration of 4000 s. For this reason, the time scale of the oscilloscope has been tuned at 400 s/div. The square waveform signals have been chosen for this investigation because they allow describing the dynamic behavior of wind energy conversion systems where the change in the operating conditions occurs quickly.

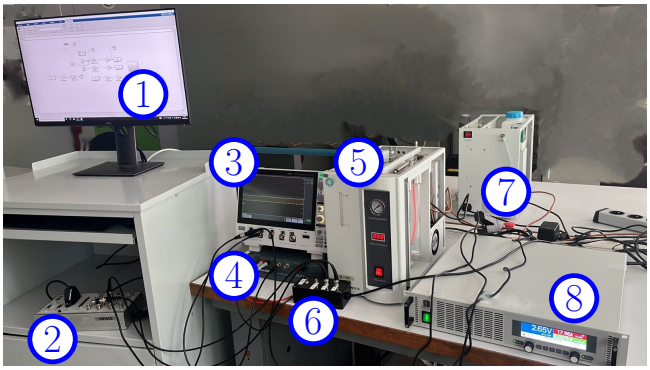

Fig. 2. Equipment and set-up to carry out the voltage and current measurements of the PEM electrolyzer.

Figures 3 and 4 show the PEM electrolyzer voltage behaviors with square waveform current input. The different square waveform current inputs were generated through Matlab–Simulink and dSPACE in a minimum step range of 0 to 10 A and a maximum step range of 7 to 20 A with switching periods of 25, 50, and 100 seconds. The different voltage responses varied between 1.6 and 2.2 V for the minimum current input steps and varied between 1.9 and 2.4 V for the maximum current input steps. The start-up voltage (red box) exhibits a different and irregular behavior compared to the regular voltage (outside the box). It is noticeable that the start-up voltage occurs when the electrolyzer starts operating (i.e., it is at room temperature and has just started operating after being shut down). The start-up voltage reported a duration time between 720 and 1800 seconds, see Figure 3. This start-up voltage is due to different factors such as cell pressure and temperature, which are variable at the beginning of the electrolyzer operation but then become constant.

In the following data collection, the electrolyzer was kept in continuous operation. Thus, the voltage presented a regular behavior, see Figure 4. This is because the different pressures and the temperature inside the cell are kept constant, and, therefore, the electric current supplied by the DC power source is the only variable parameter. After obtaining the data, the mathematical model is proposed, which is described in the next section.

III. DEVELOPMENT OF THE MATHEMATICAL MODEL

PEM electrolyzer voltage V_e can be expressed in terms of the reversible voltage V_{rev} and the three main over-voltage (ohmic V_{ohm}, activation V_{act}, and concentration V_{con}) [30]:

$$V_e = V_{rev} + V_{ohm} + V_{act} + V_{con}. \quad (2)$$

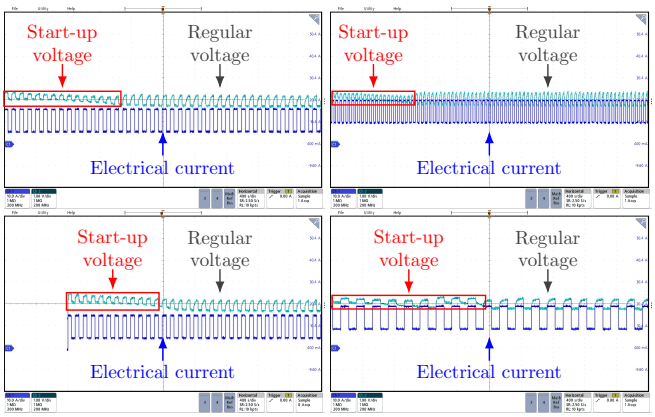

Fig. 3. Behavior of the PEM electrolyzer voltage with input square waveform electrical current (start-up voltage observation).

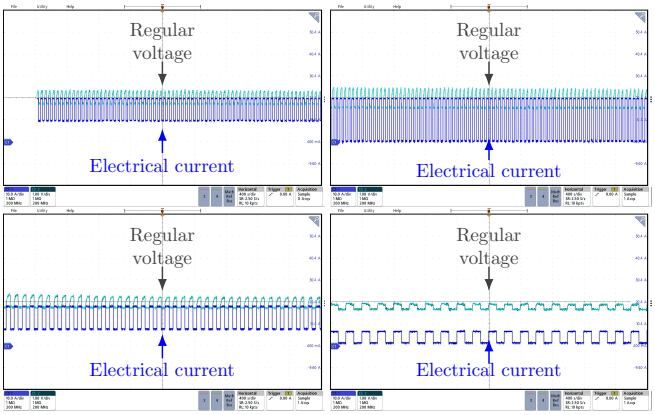

Fig. 4. Behavior of the PEM electrolyzer voltage with input square waveform electrical current (without start-up voltage observation).

Taking into consideration equation (2) and the results presented in [19], [20], a well-known ECM is presented in this section. The circuit proposed in this ECM is composed of three resistors, two capacitors, and a DC voltage source. The electronic circuit diagram is shown in Figure 5. The equivalent circuit model is developed as follows:

- The DC voltage source V_{ini} models the PEM electrolyzer reversible voltage:

$$V_{\text{rev}} = V_{\text{ini}}. \tag{3}$$

- A resistor is used to represent the resistance of the electrolyzer membrane R_{mem}, thus the ohmic over-voltage can be expressed as:

$$V_{\text{ohm}} = R_{\text{mem}} \cdot I, \tag{4}$$

where I is the PEM electrolyzer current (A).

- Two resistor-capacitor branches are used to represent the activation over-voltage. It is worth mentioning that the electrolyzer voltage dynamic occurs at this over-voltage (for both the cathode $V_{\text{act,c}}$ and the anode $V_{\text{act,a}}$).

$$V_{\text{act}} = V_{\text{act,c}} + V_{\text{act,a}}, \tag{5}$$

where the dynamic equations for $V_{\text{act,c}}$ and $V_{\text{act,a}}$ are:

$$\frac{dV_{\text{act,c}}}{dt} = \frac{1}{C_{\text{c}}} \cdot I - \frac{1}{\tau_{\text{c}}} \cdot V_{\text{act,c}}, \tag{6}$$

$$\frac{dV_{\text{act,a}}}{dt} = \frac{1}{C_{\text{a}}} \cdot I - \frac{1}{\tau_{\text{a}}} \cdot V_{\text{act,a}}, \tag{7}$$

where C_{c} and C_{a} are the capacitors for the cathode and the anode in (F), respectively. The electrical time constants τ_{c} and τ_{a} are variables that depend on the operating conditions at the cathode and the anode in (s), respectively. The resistors R_{c} and R_{a} are calculated using V_{act} and I, or using τ_{c} and τ_{a} as follows:

$$\tau_{\text{c}} = C_{\text{c}} \cdot R_{\text{c}} = C_{\text{c}} \cdot \left(\frac{V_{\text{act,c}}}{I} \right), \tag{8}$$

$$\tau_{\text{a}} = C_{\text{a}} \cdot R_{\text{a}} = C_{\text{a}} \cdot \left(\frac{V_{\text{act,a}}}{I} \right). \tag{9}$$

- The concentration over-voltage is neglected, i.e., $V_{\text{con}} = 0$. This is because the concentration over-voltage is lower compared to the ohmic and activation over-voltages [31], [32].

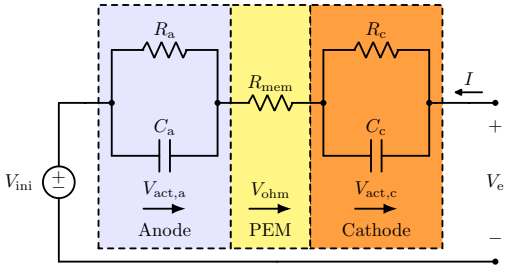

Fig. 5. Equivalent electronic circuit diagram.

So, the static-dynamic ECM for the PEM electrolyzer voltage can be expressed as:

$$V_{\text{e}}(t) = V_{\text{ini}} + R_{\text{mem}} \cdot I(t) + V_{\text{act}}(t). \tag{10}$$

To completely characterize $V_{\text{e}}(t)$, it is necessary to find the solution of the differential equations (6) and (7). Solving these differential equations employing Laplace's transform, it is obtained:

$$V_{\text{act,c}}(t) = \left(\frac{\tau_{\text{c}}}{C_{\text{c}}} \right) \mathcal{L}^{-1} \left\{ \frac{\mathcal{L}\{I(t)\}}{s \cdot \tau_{\text{c}} + 1} \right\} + V_{\text{act,c,0}} \cdot e^{\left(-\frac{t}{\tau_{\text{c}}}\right)} \tag{11}$$

$$V_{\text{act,a}}(t) = \left(\frac{\tau_{\text{a}}}{C_{\text{a}}} \right) \mathcal{L}^{-1} \left\{ \frac{\mathcal{L}\{I(t)\}}{s \cdot \tau_{\text{a}} + 1} \right\} + V_{\text{act,a,0}} \cdot e^{\left(-\frac{t}{\tau_{\text{a}}}\right)} \tag{12}$$

where $V_{\text{act,c,0}}$ and $V_{\text{act,a,0}}$ are the initial values of $V_{\text{act,c}}$ and $V_{\text{act,a}}$, respectively. Besides, as mentioned in Section II, the electrical current function used in the experiment is the square waveform function given by:

$$I(t+T) = I(t) = \begin{cases} A_1 & \text{if} \quad 0 \leq t < \frac{T}{2}, \\ A_2 & \text{if} \quad \frac{T}{2} \leq t < T, \end{cases} \tag{13}$$

where T is the period of the function in (s). Substituting (13) into (11) and (12) and applying the second Theorem of

translation, the solution for $V_{\mathrm{act,c}}$ is:

$$V_{\mathrm{act,c}} = \left(\frac{(A_1 - A_2)\tau_{\mathrm{c}}}{C_{\mathrm{c}}}\right) \cdot \sum_{k=0}^{\infty}(-1)^k \cdot U_{\frac{T\cdot k}{2}} \cdot \left(1 - e^{\left(\frac{T\cdot k - 2t}{2\tau_{\mathrm{c}}}\right)}\right) + G_1, \tag{14}$$

where

$$G_1 = \left(\frac{A_2\tau_{\mathrm{c}}}{C_{\mathrm{c}}}\right)\left(1 - e^{\left(-\frac{t}{\tau_{\mathrm{c}}}\right)}\right) + V_{\mathrm{act,c,0}} \cdot e^{\left(-\frac{t}{\tau_{\mathrm{c}}}\right)} \tag{15}$$

and $U_{\frac{T\cdot k}{2}}$ is the unitary function:

$$U_{\frac{T\cdot k}{2}} = \begin{cases} 0 & \text{if} \quad t < \frac{T\cdot k}{2}, \\ 1 & \text{if} \quad t \geq \frac{T\cdot k}{2}. \end{cases} \tag{16}$$

Similarly, the solution for $V_{\mathrm{act,a}}$ is given by:

$$V_{\mathrm{act,a}} = \left(\frac{(A_1 - A_2)\tau_{\mathrm{a}}}{C_{\mathrm{a}}}\right) \cdot \sum_{k=0}^{\infty}(-1)^k \cdot U_{\frac{T\cdot k}{2}} \cdot \left(1 - e^{\left(\frac{T\cdot k - 2t}{2\tau_{\mathrm{a}}}\right)}\right) + G_2, \tag{17}$$

where

$$G_2 = \left(\frac{A_2\tau_{\mathrm{a}}}{C_{\mathrm{a}}}\right)\left(1 - e^{\left(-\frac{t}{\tau_{\mathrm{a}}}\right)}\right) + V_{\mathrm{act,a,0}} \cdot e^{\left(-\frac{t}{\tau_{\mathrm{a}}}\right)}. \tag{18}$$

Thus, using (14) and (17), and in view of (10), a complete characterization of $V_{\mathrm{e}}(t)$ can be established for the input current function $I(t)$ given by (13).

IV. Parameter Estimation

Once the complete characterization of $V_{\mathrm{e}}(t)$ is obtained, the model parameters are calculated. To estimate the parameters, the experimental data are first analyzed. Throughout the experimental stage, seven databases are obtained with different values for A_1, A_2, T, and $V_{\mathrm{act,0}}$, see Table II.

TABLE II
SPECIFICATIONS OF THE SEVEN DATABASES OBTAINED DURING THE EXPERIMENT STAGE.

Test	A_1	A_2	T	$V_{\mathrm{act,0}}$
Test 1	20 A	10 A	50 s	0.7015 V
Test 2	20 A	1 A	50 s	0.2758 V
Test 3	5 A	15 A	50 s	0.4163 V
Test 4	6 A	16 A	100 s	0.4010 V
Test 5	18 A	8 A	100 s	0.2562 V
Test 6	9 A	19 A	200 s	0.9956 V
Test 7	2 A	7 A	200 s	0.3432 V

Figures 6 and 7 show two examples of the obtained databases. An example of the PEM electrolyzer voltage behavior when start-up voltage is presented in the experimental data (Test 6, see Table II) is shown in Figure 6. In this case, the start-up voltage time was 1800 s (30 minutes). An example of the PEM electrolyzer voltage behavior without start-up voltage (Test 7, see Table II) is shown in Figure 7. In this case, the electrolyzer voltage is regular and more uniform than in the previous example.

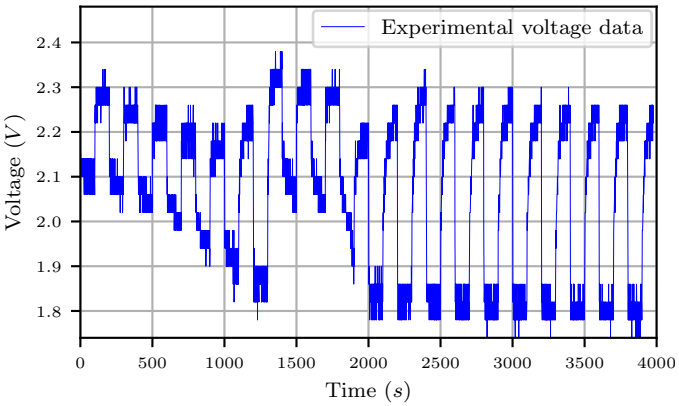

Fig. 6. PEM electrolyzer voltage behavior with start-up voltage (Test 6 database).

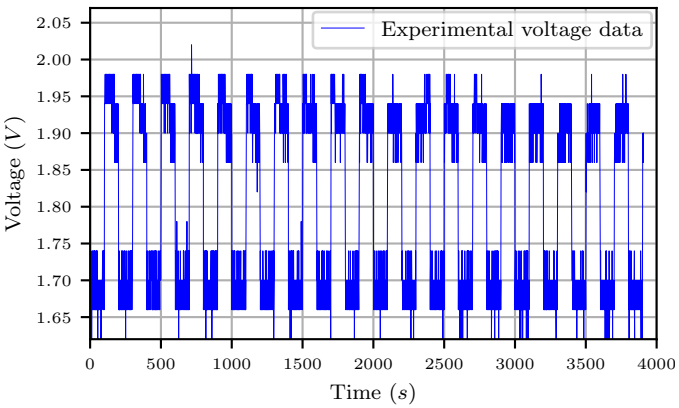

Fig. 7. PEM electrolyzer voltage behavior without start-up voltage (Test 7 database).

After data analysis, the model parameters are estimated. To ensure the accuracy of the static-dynamic ECM, a systematic parameter estimation methodology based on nonlinear curve fitting was employed. This methodology considers the decomposition of the PEM electrolyzer voltage into its ohmic, activation, and concentration components, integrated with a first-order RC network. While the activation resistance is considered a grouped parameter within the analyzed cycles, the novelty of this mathematical approach lies in the simultaneous fitting of the RC time constants, specifically under repetitive square-wave transitions. This allows the model to capture the cumulative effect of continuous disturbances on voltage transients, a feature that steady-state models cannot achieve. The parameters to be estimated are V_{ini}, R_{mem}, C_{c}, C_{a}, τ_{c}, and τ_{a}. The capacitances C_{c} and C_{a} are considered to be equal, $C_{\mathrm{c}} = C_{\mathrm{a}}$, due to the advantage of building an electronic circuit with the same capacitance. To estimate the parameters V_{ini}, R_{mem}, and C_{c}, a m-file is developed in Matlab. This m-file allows estimating parameter values for each database based on the values reported in the work [19]. The values obtained for these parameters when using the m-file for the seven different databases are shown in Table III. Hence, to assign the estimated values, the average of the obtained values is taken. As shown in Table III, $V_{\mathrm{ini}} = 1.4323$ V, $R_{\mathrm{mem}} = 0.0114$ Ω, and $C_{\mathrm{c}} = 125.0088$ F.

TABLE III
PARAMETER VALUES V_{ini}, R_{mem}, AND C_{c} FOR EACH TEST.

Test	V_{ini} (V)	R_{mem} (Ω)	C_{c} (F)
Test 1	1.1322	0.0137	154.1159
Test 2	1.4091	0.0166	117.1766
Test 3	1.5449	0.0164	159.2286
Test 4	1.4424	0.0057	113.1172
Test 5	1.4812	0.0099	112.5690
Test 6	1.4236	0.0021	117.2113
Test 7	1.5928	0.0155	101.6432
Average	1.4323	0.0114	125.0088

Using the estimated values of V_{ini}, R_{mem}, and C_{c}, the parameters τ_{c} and τ_{a} are calculated for each test, the results are presented in Table IV and 8. As can be seen in Table IV and 8, these two parameters depend on the input electrical current. It is noticeable that, for a current greater than 10 A, the parameters remain constant, and for a current between 0 and 10 A, the parameters vary significantly. This behavior in the parameters agrees with the reported works [19], [20], where the authors have developed a current-dependent function for τ_{c} and τ_{a}. In this work, for the QL-300 PEM electrolyzer, two current-dependent functions (one to estimate τ_{c} and one to estimate τ_{a}, (19)) are determined using a linear combination of Gaussian functions due to the few variations in input current values, the soft nature of these functions, low computational demand, and adaptability to accommodate new data. Figure 8 shows the behavior of the data obtained, the linear interpolation, and the interpolation using (19) for the parameters τ_{c} and τ_{a}.

TABLE IV
PARAMETER VALUES τ_{c} AND τ_{a} FOR EACH INPUT ELECTRICAL CURRENT AND TEST.

Test	I (A)	τ_{c} (s)	τ_{a} (s)
Test 1	$A_1 = 20$	3.7200	0.3070
	$A_2 = 10$	3.7200	0.3070
Test 2	$A_1 = 20$	3.7200	0.3070
	$A_2 = 1$	3.3456	0.2974
Test 3	$A_1 = 5$	3.8839	2.0441
	$A_2 = 15$	3.7200	0.3070
Test 4	$A_1 = 6$	4.5973	0.4781
	$A_2 = 16$	3.7200	0.3070
Test 5	$A_1 = 18$	3.7200	0.3070
	$A_2 = 8$	2.8454	0.5375
Test 6	$A_1 = 9$	4.3031	0.1680
	$A_2 = 19$	3.7200	0.3070
Test 7	$A_1 = 2$	1.4500	1.7360
	$A_2 = 7$	2.6681	0.1360

$$\tau_{\text{c}} = f_1(I) + f_2(I), \ \tau_{\text{a}} = g_1(I) + g_2(I), \tag{19}$$

where

$$f_1(I) = -0.5585 \exp\left[-0.4I\right] + 3.7200, \tag{20}$$
$$g_1(I) = -0.0117 \exp\left[-0.2I\right] + 0.3070, \tag{21}$$

and

$$f_2(I) = \sum_{i=1}^{3} c_i \exp\left[\frac{-(I-\mu_{\text{c,i}})^2}{2\sigma_{\text{c,i}}^2}\right], \tag{22}$$
$$g_2(I) = \sum_{i=1}^{4} d_i \exp\left[\frac{-(I-\mu_{\text{a,i}})^2}{2\sigma_{\text{a,i}}^2}\right], \tag{23}$$

with c_i =1.9388, 4.4833, 2, respectively; $\mu_{\text{c,i}}$ =7.3076, 7.4562, 2, respectively; $\sigma_{\text{c,i}}$ =1.0874, 0.4885, 0.3, respectively; d_i =1.4369, 1.7414, 0.3512, 0.5830, respectively; $\mu_{\text{a,i}}$ =2, 5, 7.9384, 8, respectively; $\sigma_{\text{a,i}}$ =0.198, 0.475, 0.7739, 0.198, respectively.

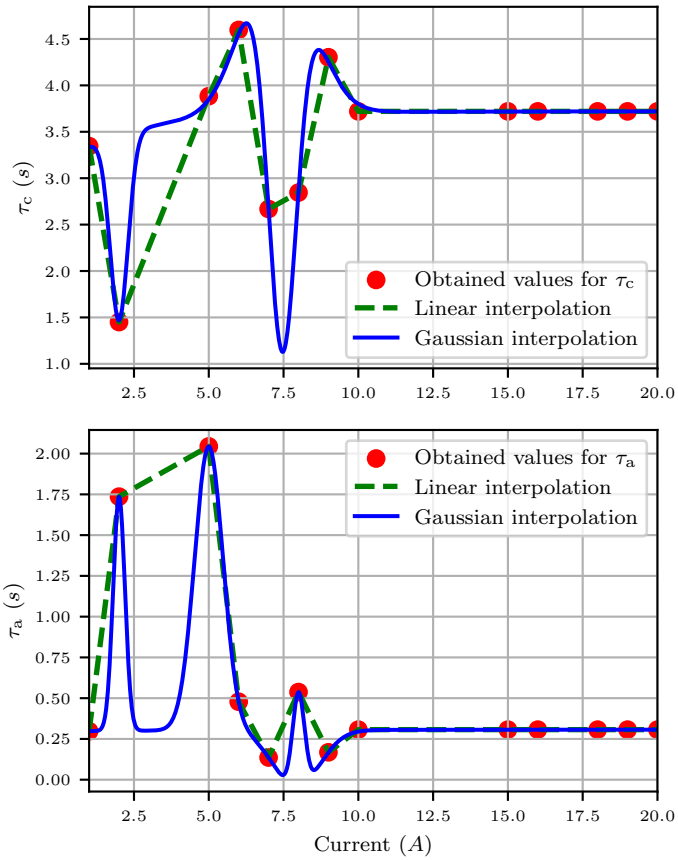

Fig. 8. Behavior of the data obtained, the linear interpolation, and the Gaussian interpolation for the parameters τ_{c} and τ_{a}.

In the next section, the numerical simulation results using the estimated parameter values are presented.

V. RESULTS AND DISCUSSION

A. Simulation and validation

In this section, numerical simulations of the proposed model are presented and analyzed using the parameter values obtained in Section IV and comparing them with the experimental data obtained in Section II. Figure 9 presents the comparison of the experimental voltage data and the model simulation for Tests 1–3 (period $T = 50$ s). As can be seen, in the database of Test 1, the phenomenon of start-up voltage during the operation of the PEM electrolyzer can be identified, while in the other two tests, the experimental voltage data maintained a regular behavior without start-up voltage.

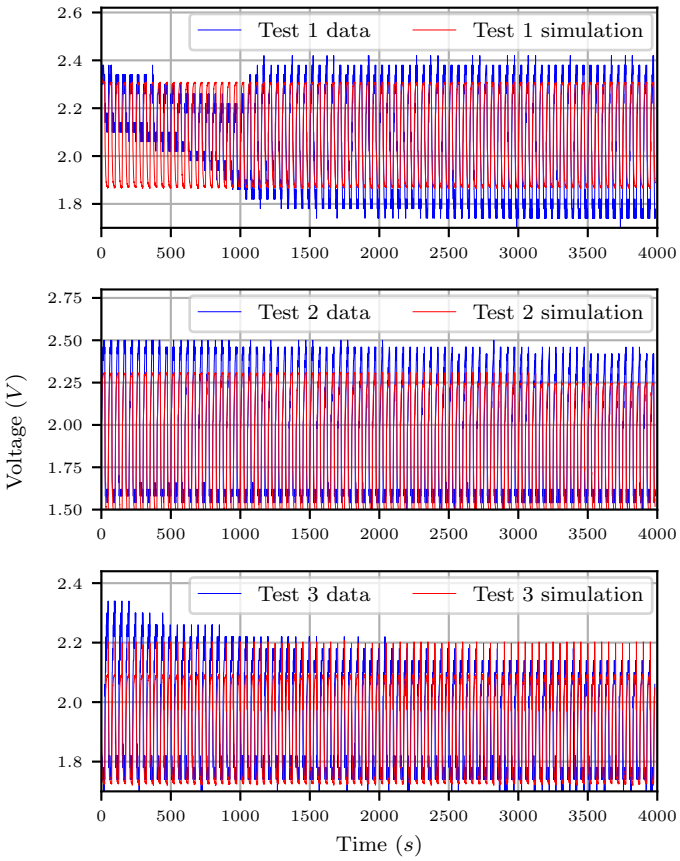

Fig. 9. Comparison of the experimental voltage data and the simulation ECM for Tests 1–3 (period $T = 50$ s).

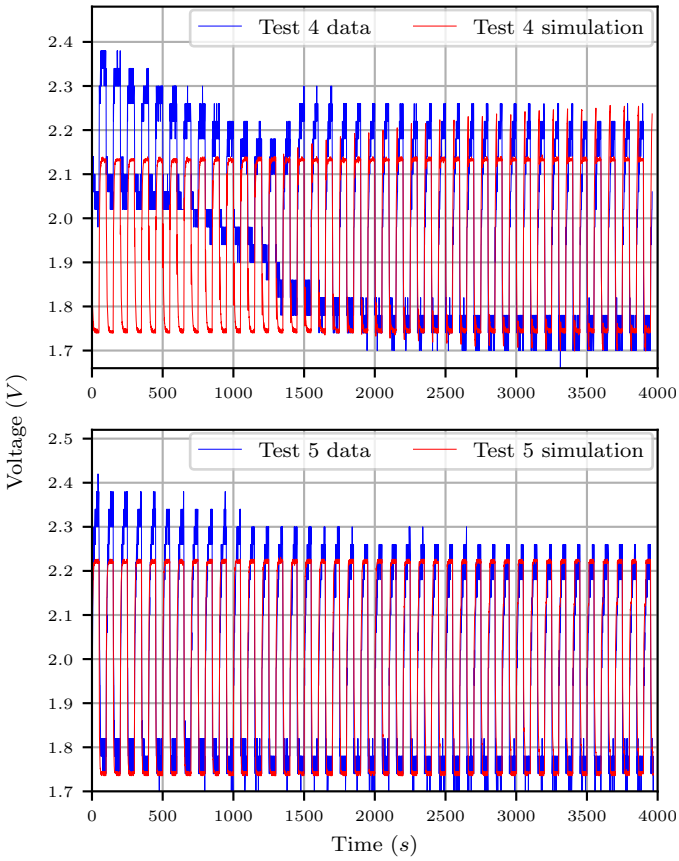

Fig. 10. Comparison of the experimental voltage data and the simulation ECM for Tests 4 and 5 (period $T = 100$ s).

Figure 10 shows the comparison of the experimental voltage data and the model simulation for Tests 4 and 5 (period $T = 100$ s). During Test 4, the start-up voltage can be observed as a result of the inactivity of the PEM electrolyzer before developing this test. The voltage data obtained in Test 5 presented a behavior without a start-up voltage in comparison to Test 4.

Figure 11 illustrates the comparison of the experimental voltage data and the model simulation for Tests 6 and 7 (period $T = 200$ s). During Test 6, the phenomenon of start-up voltage occurred similarly to Tests 1 and 4. It should be noted that in Test 6, the start-up voltage time is longer compared to Tests 1 and 4. The voltage data for Test 7, in contrast to Test 6, presented a voltage behavior without a start-up voltage.

After observing the comparisons of the experimental data with the simulations, the relative error E_{r}, mean error E_{m}, mean squared error E_{MS}, and root mean squared error E_{RMS} are calculated to formally validate the model. These statistical errors are calculated by using the following equations:

$$E_{\mathrm{r}} = \left(\frac{100}{N_d}\right) \sum_{k=1}^{N_d} \left| \frac{V_{\mathrm{exp,k}} - V_{\mathrm{sim,k}}}{V_{\mathrm{exp,k}}} \right|, \tag{24}$$

$$E_{\mathrm{m}} = \left(\frac{1}{N_d}\right) \sum_{k=1}^{N_d} \left| V_{\mathrm{exp,k}} - V_{\mathrm{sim,k}} \right|, \tag{25}$$

$$E_{\mathrm{MS}} = \left(\frac{1}{N_d}\right) \sum_{k=1}^{N_d} \left(V_{\mathrm{exp,k}} - V_{\mathrm{sim,k}} \right)^2, \tag{26}$$

$$E_{\mathrm{RMS}} = \sqrt{E_{\mathrm{MS}}}, \tag{27}$$

where N_d is the number of measurements in the database obtained in Section II: 9966 for Test 1; 9962 for Test 2; 9956 for Test 3; 9904 for Test 4; 9924 for Test 5; 9939 for Test 6; 9770 for Test 7. $V_{\mathrm{exp,k}}$ and $V_{\mathrm{sim,k}}$ are the k-th measurements in (V) for the experiment and simulation, respectively.

The results obtained from the statistical tests are shown in Table V. As can be seen, the model showed a higher accuracy for the voltage data of Test 7, having a higher performance in all the statistics tests. On the contrary, the model presented a lower precision than the voltage data of Test 2, exhibiting a lower performance in all the statistical tests. Taking into account the general accuracy of the model, the average relative error obtained is less than 5% ($E_{\mathrm{r}} = 3.5229\%$), which validates the ECM for square wave input current signals.

B. Discussion

The obtained values of the average statistical errors have demonstrated the validity of the proposed ECM for the PEM electrolyzer voltage when subjected to square wave input current signals, see Table V. Besides, the square waveform

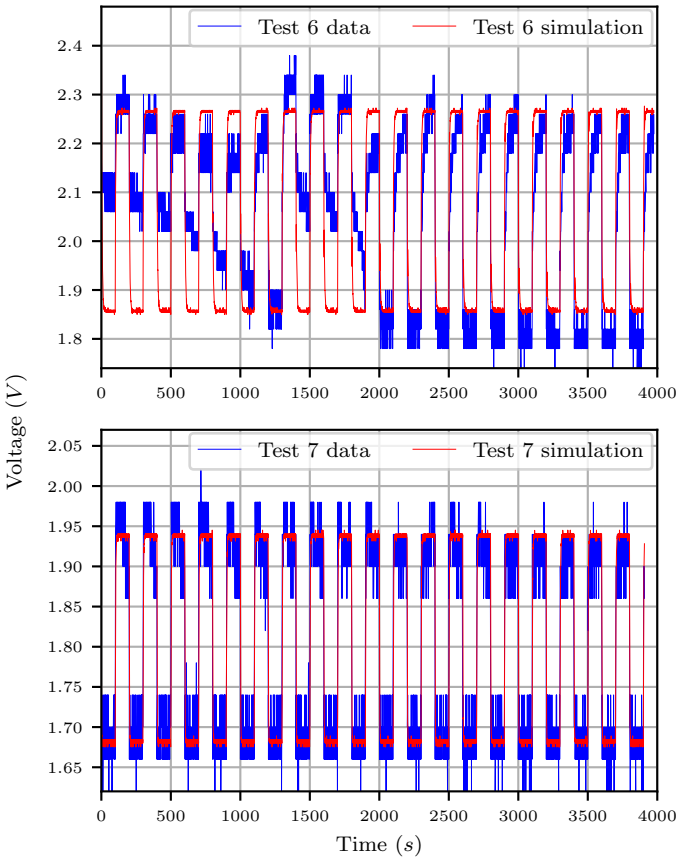

Fig. 11. Comparison of the experimental voltage data and the simulation model for Tests 6 and 7 (period $T = 200$ s).

TABLE V
RESULTS OF THE STATISTICAL TESTS.

Test	E_{r} (%)	E_{m} (V)	E_{MS} (V^2)	E_{RMS} (V)
Test 1	3.4562	0.0695	0.0077	0.0875
Test 2	5.3882	0.1004	0.0136	0.1167
Test 3	3.4112	0.0667	0.0088	0.0937
Test 4	4.6657	0.0962	0.0173	0.1316
Test 5	2.2313	0.0441	0.0039	0.0624
Test 6	4.0170	0.0824	0.0116	0.1078
Test 7	1.4908	0.0269	0.0013	0.0360
Average	3.5229	0.0695	0.0092	0.0908

input electrical current applied in this investigation allows studying the effect of continuous disturbances during the operation of the PEM electrolyzer. However, even though the model has proven its efficiency in simulating the PEM electrolyzer voltage, the model can achieve higher performance by taking into account the variables that cause the start-up voltage phenomenon reported in the experimental part of this work, see Table VII. Besides, the proposed ECM only considers the input current and the values of the components of an electronic circuit, which has a high level of accuracy when the PEM electrolyzer voltage does not present the start-up voltage, see Table VII. Furthermore, when the obtained errors are analyzed (Figures 12–13), the impact that the start-up voltage has on the accuracy of the model can be appreciated. Figures 12–13 show the behavior of the error for tests with period $T = 50$ s, $T = 100$ s, and $T = 200$ s, respectively. As can be seen, the error behaviors of Test 1 (Figure 12), Test 4 (Figure 13), and Test 6 (Figure 14) are more complex to interpret compared to the other tests due to the influence that the start-up voltage had on these data and the relative error at this stage can reach up to 7.9610% and on average 5.8935% (Table VI). For this reason, the start-up voltage factor must be considered to improve the ECM used in this work. Furthermore, to model the start-up voltage phenomenon efficiently, different factors present in the PEM electrolyzer must be taken into consideration, such as temperature, and pressure at the anode and cathode, which significantly influence the initial stage of operation of the PEM electrolyzer. However, as can be seen in Figures 12–14, these factors stop significantly influencing the voltage behavior of the PEM electrolyzer after a period of operation, reaching a regular voltage behavior, i.e., the voltage response only depends directly on the input current and the relative error, taking into account only this stage, can reach up to 3.0378% (for all the test 5.3882%) and on average 2.9011% (for all the test 3.0321%), Table VI. Therefore, the proposed ECM is optimized for dynamic steady-state operation, which is the most relevant state for studying power electronics interfaces and microgrids operating for extended periods. One way to analytically improve the ECM proposed in this work is by considering, in initial operation, the electrolyzer voltage as a function of current, temperature, and pressure, and after a period of operation, treating the electrolyzer voltage as a function of current only. Another way to improve the ECM based on error curves is to develop an empirical model for the error $e(t)$ resulting from the comparison of the ECM proposed and the experimental voltage data, $e(t) \approx V_{\mathrm{exp}} - V_{\mathrm{sim}}$. Thus, as future work, a new model for the PEM electrolyzer voltage is expressed as $V(t) = V_{\mathrm{e}} + e(t)$, where V_{e} is the voltage obtained by the ECM.

TABLE VI
RESULTS OF THE STATISTICAL TESTS FOR TEST WITH START-UP VOLTAGE (START-UP PHASE).

Test	E_{r} (%)	E_{m} (V)	E_{MS} (V^2)	E_{RMS} (V)
Test 1	4.7058	0.0996	0.0158	0.1256
Test 4	7.9610	0.1664	0.0372	0.1928
Test 6	5.0137	0.1050	0.0174	0.1318
Average	5.8935	0.1237	0.0235	0.1501

TABLE VII
RESULTS OF THE STATISTICAL TESTS FOR TEST WITH START-UP VOLTAGE (REGULAR OPERATION).

Test	E_{r} (%)	E_{m} (V)	E_{MS} (V^2)	E_{RMS} (V)
Test 1	3.0378	0.0594	0.0049	0.0703
Test 4	2.6576	0.0534	0.0052	0.0723
Test 6	3.0080	0.0595	0.0058	0.0760
Average	2.9011	0.0574	0.0053	0.0729

The ECM proposed in this work is a fundamental tool for designing control strategies. In particular, as a future line of research, it is possible to propose a control strategy that smooths the input current by limiting its rate of change, leveraging the model's ability to predict voltage transients and the state of the double-layer capacitance. This approach would

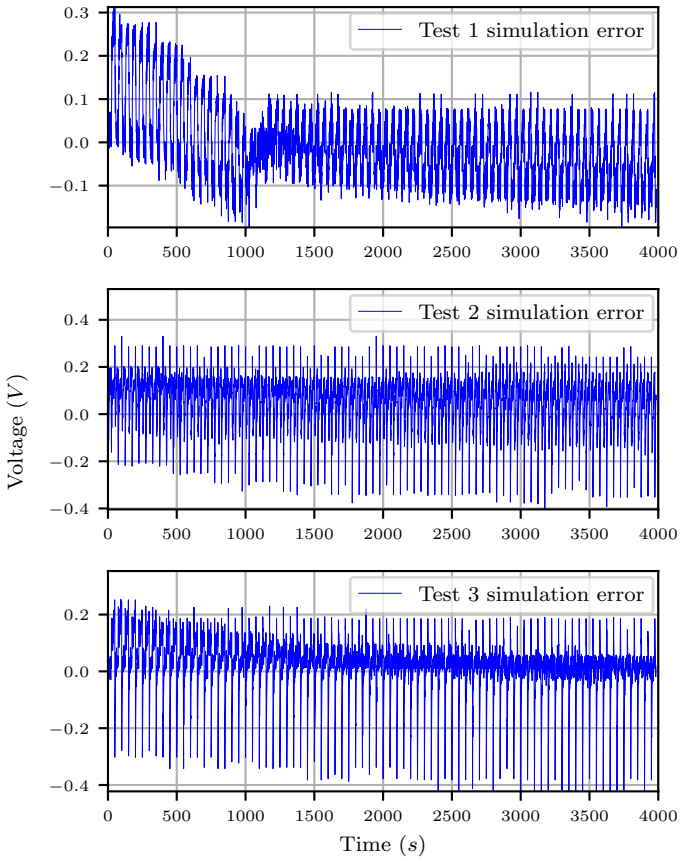

Fig. 12. Behavior of the error obtained for Tests 1–3 (period $T = 50$ s).

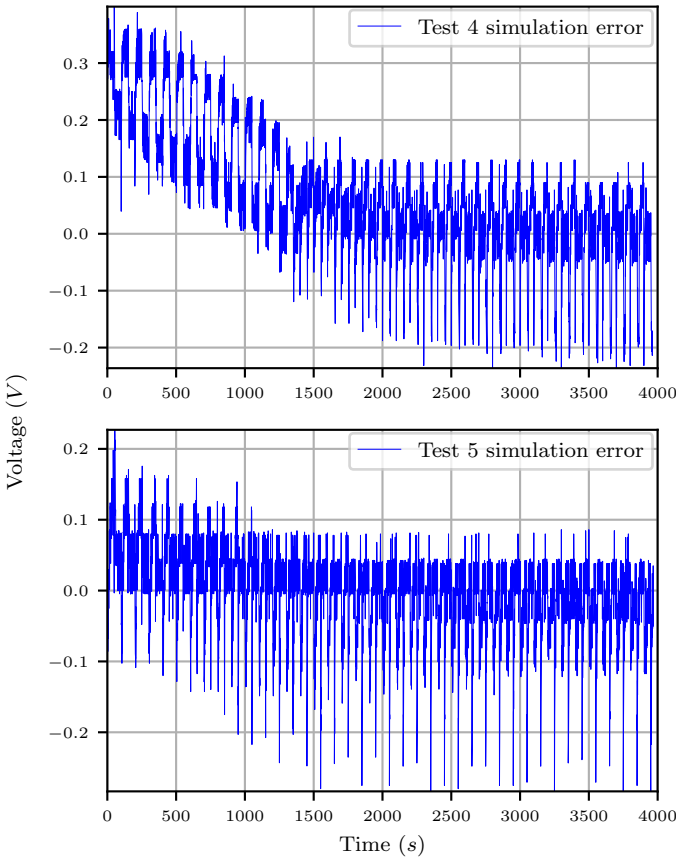

Fig. 13. Behavior of the error obtained for Tests 4 and 5 (period $T = 100$ s).

mitigate the sharp voltage spikes observed during on/off cycles, thereby reducing mechanical and thermal stress on the PEM membrane and potentially extending the electrolyzer's lifespan when integrated with fluctuating power sources. Besides, the ECM analyzed in this work is scalable, making it suitable for commercial applications ranging from kW to MW. The model parameters can be adjusted to represent a full cell stack by applying scaling factors based on the number of cells in series and their active area. For large-scale implementation, the main technical challenge lies in thermal management and the non-uniform current distribution across the stack under fast transients. The ECM proposed can reduce costs by enabling optimized design of power electronics and balance-of-plant components, avoiding oversizing of filters and protection equipment.

VI. Conclusion

In this work, the use of square-wave electrical currents has enabled a comprehensive study of the PEM electrolyzer voltage behavior under continuous and rapid perturbations. This approach reveals the complex interaction between double-layer capacitance and charge transfer resistance during repetitive switching cycles. The results demonstrate that the proposed ECM is capable of accurately capturing these transient effects, which are often overlooked in steady-state modeling. Consequently, this analysis provides a solid foundation for future work, where the efficiency and reliability of power converters can be optimized by adapting control strategies to the specific dynamic limitations and capabilities of the observed PEM electrolyzer. This is relevant for improving the lifetime and performance of hydrogen production systems coupled with intermittent renewable energy sources. Furthermore, for applications where the start-up of the PEM electrolyzer is critical (such as ultra-fast response systems in extreme climates), the proposed ECM must be complemented with a thermal network.

References

[1] Y. Liu, R. Wang, R. Li, W. Feng, H. H. C. Iu, T. Fernando, and X. Zhang, "A novel neural network-based control method for proton exchange membrane fuel cell in dc microgrids," *IEEE Journal of Emerging and Selected Topics in Industrial Electronics*, vol. 6, no. 4, pp. 1319–1328, 2025.

[2] Y. Wu, X. Pan, L. Yang, H. Yuan, and Z. Cai, "Asymmetric phase shift control in multiphase dual active bridge dc/dc converters," *IEEE Journal of Emerging and Selected Topics in Industrial Electronics*, vol. 6, no. 4, pp. 1271–1283, 2025.

[3] E. Escobedo, D. García, M. Ruiz, A. Izquierdo, D. Pacheco-Catalán, and L. Ordóñez, "Design, construction, and performance of a próton exchange membrane water electrolyzer (pem-we)," *International Journal of Electrochemical Science*, vol. 18, no. 5, p. 100110, 2023.

[4] F. Gutiérrez-Martín, L. Amodio, and M. Pagano, "Hydrogen production by water electrolysis and off-grid solar pv," *International Journal of Hydrogen Energy*, vol. 46, no. 57, pp. 29 038–29 048, 2021.

[5] R. R. Kar and R. Wandhare, "Enhanced stability and control of voltage source converters with lcl filter in weak grid," *IEEE Journal of Emerging and Selected Topics in Industrial Electronics*, vol. 6, no. 1, pp. 271–283, 2025.

[6] N. Shakeri, M. Zadeh, and J. Bruinsma, "Dynamic modeling and validation of a fuel cell-based hybrid power system for zero-emission marine propulsion: An equivalent circuit model approach," *IEEE Journal*

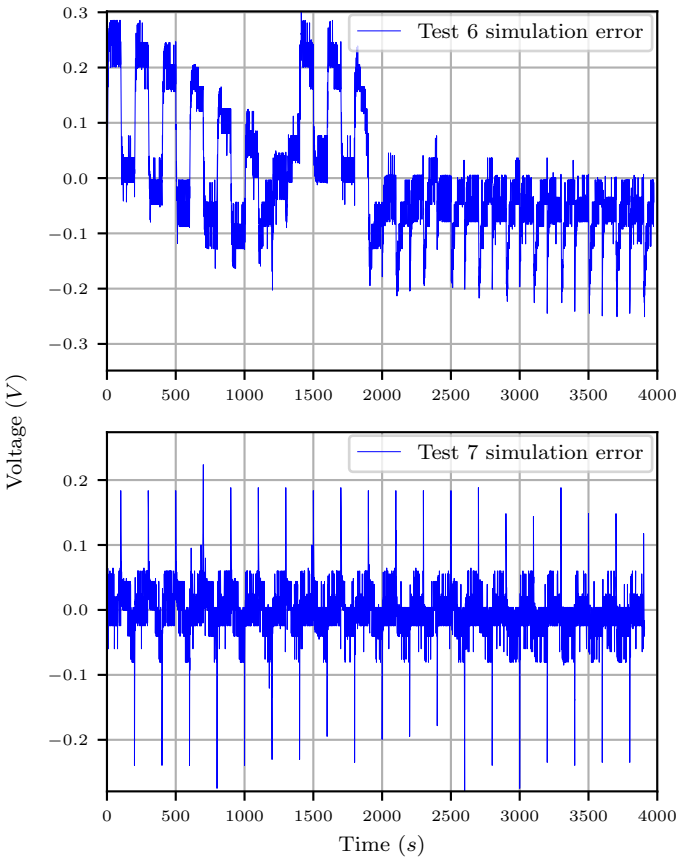

Fig. 14. Behavior of the error obtained for Tests 6 and 7 (period $T = 200$ s).

of Emerging and Selected Topics in Industrial Electronics, vol. 5, no. 3, pp. 1065–1079, 2024.

[7] S. Becker and V. Karri, "Predictive models for pem-electrolyzer performance using adaptive neuro-fuzzy inference systems," *International Journal of Hydrogen Energy*, vol. 35, no. 18, pp. 9963–9972, 2010.

[8] B. Wang, M. Ni, S. Zhang, Z. Liu, S. Jiang, L. Zhang, F. Zhou, and K. Jiao, "Two-phase analytical modeling and intelligence parameter estimation of proton exchange membrane electrolyzer for hydrogen production," *Renewable Energy*, vol. 211, pp. 202–213, 2023.

[9] F. J. Folgado, I. González, and A. J. Calderón, "Pem electrolyzer digital replica based on internal resistance determination applied to hydrogen energy storage," *Journal of Energy Storage*, vol. 75, p. 109694, 2024.

[10] L. Järvinen, P. Puranen, A. Kosonen, V. Ruuskanen, J. Ahola, P. Kauranen, and M. Hehemann, "Automized parametrization of pem and alkaline water electrolyzer polarisation curves," *International Journal of Hydrogen Energy*, vol. 47, no. 75, pp. 31 985–32 003, 2022.

[11] A. Abdol Rahim, A. S. Tijani, S. Kamarudin, and S. Hanapi, "An overview of polymer electrolyte membrane electrolyzer for hydrogen production: Modeling and mass transport," *Journal of Power Sources*, vol. 309, pp. 56–65, 2016.

[12] M. Espinosa-López, C. Darras, P. Poggi, R. Glises, P. Baucour, A. Rakotondrainibe, S. Besse, and P. Serre-Combe, "Modelling and experimental validation of a 46 kw pem high pressure water electrolyzer," *Renewable Energy*, vol. 119, pp. 160–173, 2018.

[13] V. Martinez Lopez, H. Ziar, J. Haverkort, M. Zeman, and O. Isabella, "Dynamic operation of water electrolyzers: A review for applications in photovoltaic systems integration," *Renewable and Sustainable Energy Reviews*, vol. 182, p. 113407, 2023.

[14] O. Atlam and M. Kolhe, "Equivalent electrical model for a proton exchange membrane (pem) electrolyser," *Energy Conversion and Management*, vol. 52, no. 8, pp. 2952–2957, 2011.

[15] J. van der Merwe, K. Uren, G. van Schoor, and D. Bessarabov, "A study of the loss characteristics of a single cell pem electrolyser for pure hydrogen production," in *2013 IEEE International Conference on Industrial Technology (ICIT)*, 2013, pp. 668–672.

[16] C. Martinson, G. van Schoor, K. Uren, and D. Bessarabov, "Characterisation of a pem electrolyser using the current interrupt method," *International Journal of Hydrogen Energy*, vol. 39, no. 36, pp. 20 865–20 878, 2014.

[17] C. Rozain and P. Millet, "Electrochemical characterization of polymer electrolyte membrane water electrolysis cells," *Electrochimica Acta*, vol. 131, pp. 160–167, 2014, electrochemical Impedance Spectroscopy.

[18] D. Guilbert and G. Vitale, "Dynamic emulation of a pem electrolyzer by time constant based exponential model," *Energies*, vol. 12, no. 4, 2019.

[19] A. Hernández-Gómez, V. Ramirez, D. Guilbert, and B. Saldivar, "Development of an adaptive static-dynamic electrical model based on input electrical energy for pem water electrolysis," *International Journal of Hydrogen Energy*, vol. 45, no. 38, pp. 18 817–18 830, 2020.

[20] ——, "Cell voltage static-dynamic modeling of a pem electrolyzer based on adaptive parameters: Development and experimental validation," *Renewable Energy*, vol. 163, pp. 1508–1522, 2021.

[21] D. Guilbert, D. Sorbera, and G. Vitale, "A stacked interleaved dc-dc buck converter for proton exchange membrane electrolyzer applications: Design and experimental validation," *International Journal of Hydrogen Energy*, vol. 45, no. 1, pp. 64–79, 2020.

[22] Z. Gao and Y. Tian, "Self-sustaining control strategy for proton-exchange membrane electrolysis devices based on gradient-disturbance observation method," *Processes*, vol. 11, no. 3, 2023.

[23] K.-C. Tseng, H.-L. Hsu, Y.-H. Su, and C.-A. Cheng, "A novel isolated high-step-up interleaved converter for renewable energy systems," *IEEE Journal of Emerging and Selected Topics in Industrial Electronics*, vol. 4, no. 4, pp. 1235–1243, 2023.

[24] I. Dincer and A. A. AlZahrani, "4.25 electrolyzers," in *Comprehensive Energy Systems*, I. Dincer, Ed. Oxford: Elsevier, 2018, pp. 985–1025.

[25] D. Falcão and A. Pinto, "A review on pem electrolyzer modelling: Guidelines for beginners," *Journal of Cleaner Production*, vol. 261, p. 121184, 2020.

[26] F. STORE. (2026) Ql–300 hydrogen generator. [Online]. Available: https://www.fuelcellstore.com/pem-hydrogen-generator-ql-300

[27] S. Mucci, A. Mitsos, and D. Bongartz, "Power-to-x processes based on pem water electrolyzers: A review of process integration and flexible operation," *Computers & Chemical Engineering*, vol. 175, p. 108260, 2023.

[28] M. Langemann, D. L. Fritz, M. Müller, and D. Stolten, "Validation and characterization of suitable materials for bipolar plates in pem water electrolysis," *International Journal of Hydrogen Energy*, vol. 40, no. 35, pp. 11 385–11 391, 2015.

[29] L. Shandong Saikesaisi Hydrogen Energy Co. (2007) Hydrogen generator ql-300. [Online]. Available: http://www.ql-spe.com/enportal/Article/index.html?cid=66{\&}id=253

[30] A. Hernández-Gómez, V. Ramirez, and D. Guilbert, "Investigation of pem electrolyzer modeling: Electrical domain, efficiency, and specific energy consumption," *International Journal of Hydrogen Energy*, vol. 45, no. 29, pp. 14 625–14 639, 2020.

[31] H. Görgün, "Dynamic modelling of a proton exchange membrane (pem) electrolyzer," *International Journal of Hydrogen Energy*, vol. 31, no. 1, pp. 29–38, 2006.

[32] A. Ursúa, L. Marroyo, E. Gubía, L. M. Gandía, P. M. Diéguez, and P. Sanchis, "Influence of the power supply on the energy efficiency of an alkaline water electrolyser," *International Journal of Hydrogen Energy*, vol. 34, no. 8, pp. 3221–3233, 2009.